

# Neutron Radiography Analysis of a Transient Liquid Phase Joint

H. Ballhausen,<sup>1</sup> H. Abele,<sup>1</sup> R. S. Eccleston,<sup>2</sup> R. Gähler,<sup>3</sup> A. J. Smith,<sup>2</sup> A. Steuwer,<sup>4</sup> and A. Van Overberghe<sup>1,3</sup>

<sup>1</sup>*Physical Institute, University of Heidelberg, Philosophenweg 12, 69120 Heidelberg, Germany\**

<sup>2</sup>*Materials and Engineering Research Institute, Sheffield Hallam University, Sheffield, UK*

<sup>3</sup>*Institut Laue Langevin, 6 rue Jules Horowitz BP 156, 38042 Grenoble Cedex 9, France*

<sup>4</sup>*FaME38 at the ESRF-ILL, 6 rue Jules Horowitz, 38042 Grenoble Cedex 9, France*

Neutron radiography in many cases is the only non-destructive technique available for the analysis of a wide range of samples from metallurgy, materials engineering and materials testing. In this paper the potential of the technique is illustrated for a transient liquid phase (TLP) joint. TLP bonding produces interface free and stress free joints. The quality and properties of the joint depend on the diffusion of an interlayer into the base material. A TLP joint is visualised and the diffusion profile of the boron contained in the bonding additives is determined. Parameters of the bonding process are determined quantitatively from this profile, and flaws in the joint are detected.

## I. INTRODUCTION

Neutron radiography [1, 2, 3, 4] is a non-destructive technique and produces attenuation images similar to X-ray methods. Neutrons have the advantage over X-rays that they easily penetrate metals while showing characteristic cross-sections for different elements. With this complementary and unique probe neutron radiography is able to resolve sub- $10^{-3}$  variations of contrast on a sub-millimeter scale. In this paper we report the first demonstration of a non-destructive quantitative method for the analysis of a TLP joint.

Transient liquid phase bonding [5] is an advanced bonding technique. In most simple terms, the bonding process works as follows: A thin foil is placed between the surfaces to be bonded. It contains melting point depressants which lower the melting point of the base material. At constant temperature those parts of the assembly are liquid where the concentration of the additive is above a certain threshold. As the additive diffuses into the base material the liquid phase extends, hence the name of the method. When through diffusion the overall concentration of the additive falls below the threshold the material undergoes isothermal solidification.

TLP joints (see fig. 1) are interface free and virtually stress free due to their isothermal creation. The more even the diffusion of the additive is, and the lower its final concentration, the closer are the properties of the joint to those of the base material. Only then has the joint favourable mechanical properties, whereas regions of higher concentration of the additive are prone to embrittlement through secondary phases. It would therefore be highly advantageous to be able to quantitatively measure the spatial distribution of the additives around the joint.

Traditional metallographic (destructive) characterisation techniques cannot reveal this distribution for an individual specimen [6]. Upon interruption of the bonding process, the sample is cut to investigate the cross-section using optical methods. The phases can be distinguished by a microscope, but it is very difficult to obtain a quantitative, rather than a qualitative diffusion profile. This time consuming method has to be repeated several times to get a time resolved analysis of the bonding process.

In contrast neutron radiography delivers a visualisation of the diffusion profile (see fig. 2) within milliseconds at any stage of the bonding process without altering the sample or interfering with the process.

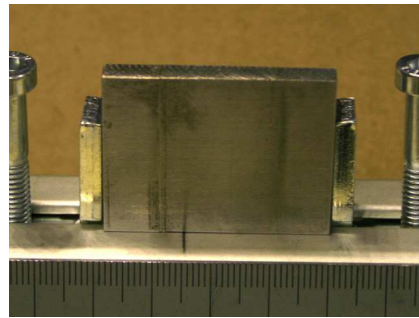


Fig. 1: sample featuring a TLP joint

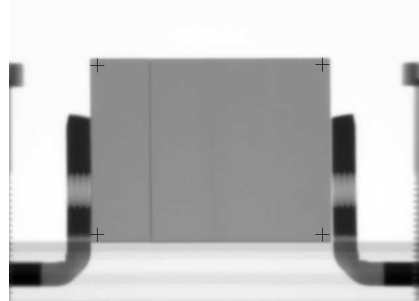


Fig. 2: neutron radiography image of the sample in fig. 1

## II. TRANSIENT LIQUID PHASE BONDING

Consider the binary phase diagram shown in figure 3. It describes the phase states of a two component alloy. This may vary in composition from pure base material (B, right) to pure additives (A, left).

In this case the additives lower the melting point of the base material. Temperature is shown on the vertical axis. As one can see the composition can be solid and liquid at the same temperature depending on the concentration of the additive within the base material.

Consider two isothermal processes which transform the alloy from one phase into another:

1. Assume that a solid piece of A is embodied in B. At its surface there is a steep concentration gradient. Solid state diffusion of A into B will create a gradient between the liquid  $C_{\alpha L}$  and  $C_{L\alpha}$ . The liquid phase around B will further dissolve the remaining solid B. This process is the isothermal solution of A (left arrow).

2. Another process is the isothermal solidification of B (right arrow). Here B diffuses into an A-rich liquid until its concentration falls below the critical liquidus  $C_{\beta L}$ .

TLP bonding consists of a combination of three such equithermal processes: liquidification of A and B and solidification of B. A thin layer of A (typically  $20\mu m \dots 50\mu m$ ) is placed between the two pieces of B to be bonded. The assembly is heated to typically  $800^\circ C \dots 1300^\circ C$ . Due to surface interdiffusion there are two thin liquid layers between the four surfaces between the three bodies (figure 4a). The following bonding process is ideally divided into three stages:

Thermodynamic forces will act to level the steep gradient of concentration within the liquid layers. At their border additional material is dissolved and enters the liquid phase to keep the concentrations  $C_{L\alpha}$  and  $C_{L\beta}$  respectively at the border of the liquid constant. This stage is called dissolution of the interlayer and is typically completed within some seconds (figure 4b).

After the interlayer has been completely dissolved the liquid phase continues to extend outwards. The concentration may now fall below  $C_{L\alpha}$  everywhere in the liquid phase and the concentration gradient will eventually level and settle down at  $C_{L\beta}$ . The lower gradient slows down this second stage considerably which typically takes some minutes (figure 4c).

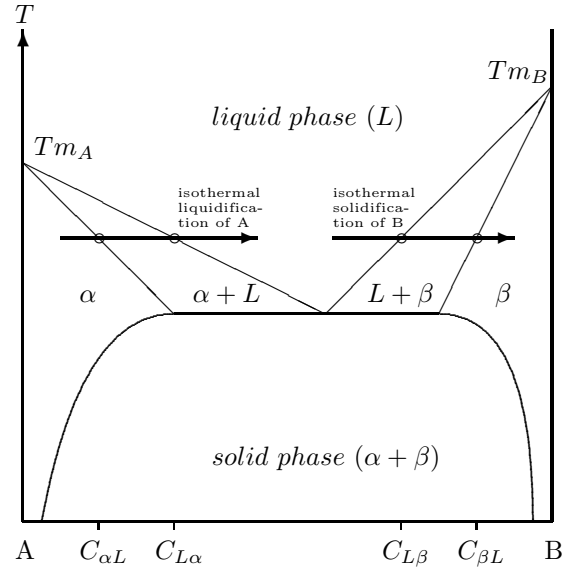


Fig. 3: binary phase diagram (horizontal axis: percentage of (A)dditive vs. (B)ase material, vertical axis: temperature)

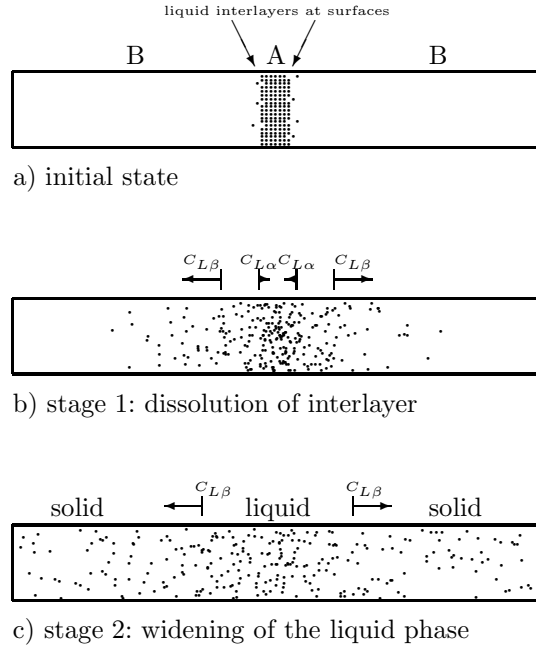
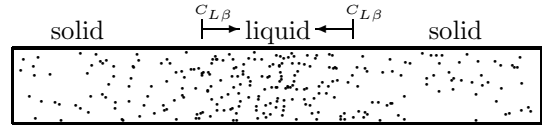


Fig. 4: transient liquid phase bonding

During the third stage additives will continue to diffuse out of the liquid into B but this solid state diffusion is a much slower process. The border of the liquid now moves inwards as the concentration of the additive falls below  $C_{L\beta}$  (figure 4d). After typically some hours the joint finally solidifies completely. Only a small concentration gradient remains.

After this bonding process there is a long period of solid state homogenization through diffusion. It may happen at bonding temperature or at room temperature and takes place on a long timescale. In practice the four stages of the process are not that ideally separated as presented here.



d) stage 3: isothermal solidification

Fig. 4: transient liquid phase bonding (continued)

### III. SAMPLE PREPARATION

A sample featuring a TLP bond was provided by The Welding Institute in Abington, UK. The sample under investigation was produced as part of a trial to optimise the process parameters of TLP bonding in terms of brazing temperature and time at temperature. This sample had been heated to  $1150^{\circ}\text{C}$  which is below the recommended brazing temperature for this foil ( $1195^{\circ}\text{C}$ ). As a result the sample features a frozen unfinished joint.

The foil used for bonding was a grade MBF-51. Its chemical composition is 15% Cr, 7.25% Si, 1.4% B, 0.06% C (in wt.%) and the balance is Ni. Both the Si and the B are the melting point depressants - they are both about as effective as each other as temperature depressants. MBF-51 is an amorphous foil - its liquidus is  $1126^{\circ}\text{C}$  - its solidus is  $1030^{\circ}\text{C}$  and the recommended braze temperature is  $1195^{\circ}\text{C}$ . The base material of the specimen was steel. The grade of steel was a 50D (S355J2G3) with a chemical composition of 0.22% C, 0.55% Si, 1.6% Mn, 0.035% P and 0.035% S.

A neutron beam penetrating the sample of thickness  $\Delta z = 0.5\text{cm}$  is attenuated by capture and incoherent scattering according to  $-\log(I/I_0) = \mu \cdot \Delta z$ . The expected attenuation coefficient for steel is  $\mu_{\text{steel}} = 1.20\text{cm}^{-1}$ . The attenuation is dominated by the capture and scattering on iron ( $\mu_{\text{Fe},sc} = 0.96\text{cm}^{-1}$ ,  $\mu_{\text{Fe},ab} = 0.21\text{cm}^{-1}$ ) which together amount for 98% of the attenuation. The foil has a higher attenuation of  $\mu_{\text{foil}} \approx 7\text{cm}^{-1}$ , dominated by capture in boron ( $\mu_{\text{B},ab} = 5.3\text{cm}^{-1}$ ) and scattering on Nickel ( $\mu_{\text{Ni},sc} = 1.3\text{cm}^{-1}$ ).

The bonding profile consisted of heating from room temperature to  $1000^{\circ}\text{C}$  at  $7.5^{\circ}\text{C min}^{-1}$  and dwell for  $5\text{min.}$ ,  $1000^{\circ}\text{C}$  to  $1150^{\circ}\text{C}$  at  $5^{\circ}\text{C min}^{-1}$  and dwell for  $15\text{min.}$ , and of cooling from  $1150^{\circ}\text{C}$  to room temperature at  $5^{\circ}\text{C min}^{-1}$ . A load of  $5\text{kN}$  was applied on the heating cycle at  $1000^{\circ}\text{C}$  and removed when the temperature fell below  $1000^{\circ}\text{C}$  on the cooling cycle. The whole process was carried out in a vacuum at  $10^{-4}\text{mbar}$ .

After the center TLP bond was finished, two cut-offs have been made on the right and on the left of the sample using a spark erosion machine. Their surfaces are level to about  $15\mu\text{m} \pm 5\mu\text{m}$ . The left gap contains a bonding foil and the right gap is empty.

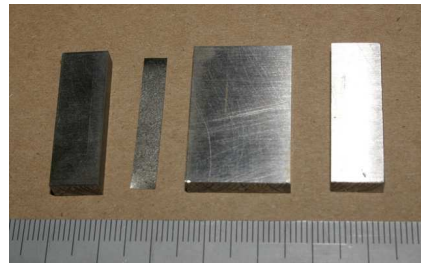


Fig. 5: preparation of the sample (l. to r.: steel, bonding foil, steel containing TLP bond, steel)

#### IV. EXPERIMENTAL SETUP

The neutron radiography station is located at the high-flux research reactor of the Institut Laue-Langevin in Grenoble, France [4, 7]. Free neutrons are produced in a fission reactor and enter the experimental area through a free flight tube. In a distance of  $15m$  from the reactor core there is a thermal neutron flux of  $3 \cdot 10^9 s^{-1} cm^{-2}$ . The beam is about  $16cm$  by  $18cm$  wide and has a divergence of less than  $0.5^\circ$ . For the purpose of this paper the beam may be treated as perfectly parallel.

The sample under investigation is placed in front of the beam window and attenuates the neutron beam. While X-rays interact electromagnetically with the electron shells in the atoms neutrons only interact strongly upon collision with a nucleus. Therefore the cross-section of neutrons does not rise with the fourth power of the element number as in the case of X-rays but rather shows an irregular pattern depending on the scattering or capturing isotope. This is why many heavy elements such as metals which are opaque to X-rays can be easily penetrated with neutrons.

For the investigation of the TLP joint use is made of the fact that the bonding interlayer contains 1.4% of boron which heavily absorbs neutrons [8].

The neutrons which are neither scattered out of the beam nor absorbed in the sample hit a detector. On a scintillator they produce light via a  $(n,\alpha)$ -reaction. The image is captured through mirrors and optics by a sensitive charge coupled device (CCD)-camera [9]. The resulting two-dimensional greyscale map is a representation of the density distribution of absorbing and scattering nuclei inside the sample.

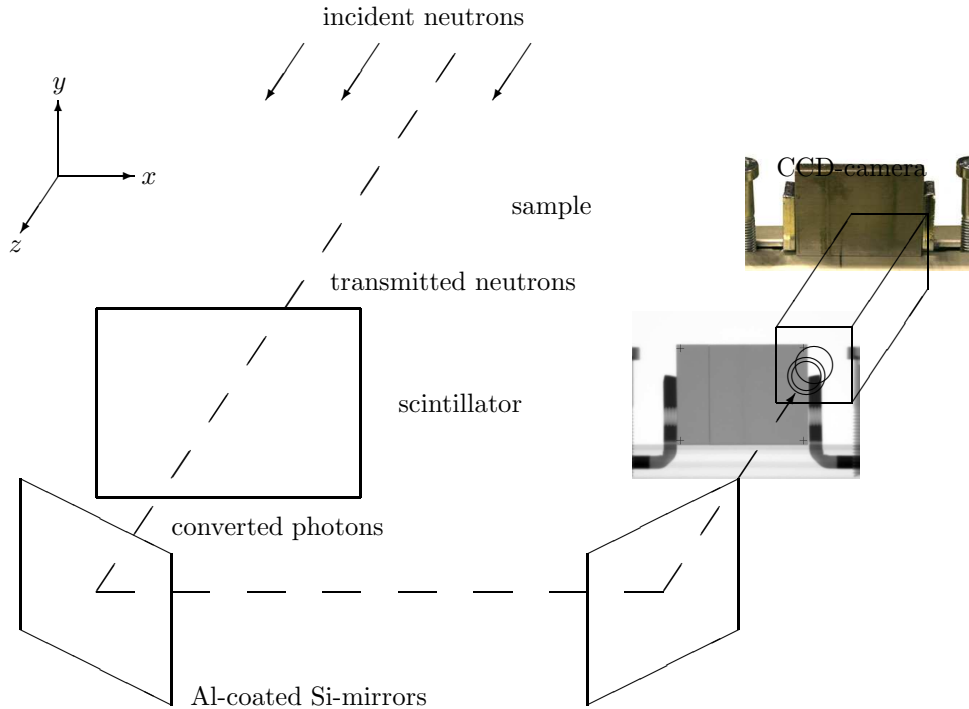


Fig. 6: neutron radiography setup

The attenuation can be calculated from the decrease in intensity according to the law of exponential attenuation  $I = I_0 \cdot \exp - \int \mu ds$ . Here we assume that  $\mu$  is independent of  $z$ . The resulting map  $\mu(x, y)$  is the neutron radiography image of the sample. In case of non-flat specimen, neutron tomography can also reveal the complete three-dimensional attenuation distribution.

## V. DATA TREATMENT AND CORRECTIONS

Figure 2 shows the neutron radiography of a stainless steel sample. The sample is 39mm by 30mm in size and is clamped to a sample holder.

The image has been corrected for the inhomogeneity of the neutron beam intensity, the inhomogeneous detector sensitivities and detector offset.

For the analysis the rectangular region indicated by the crosses was selected. On a different scale of grey-levels three vertical lines become visible in figure 7. These lines indicate the location of three cut-offs:

The center cut contains a transient liquid phase bond. Before heat treatment the interlayer foil was  $50\mu\text{m}$  thick. The increase in neutron attenuation compared to that of the steel is almost completely due to its boron content.

The left and right gap provide the reference values for the bonding foil in its initial state and for air in comparison to the diffusion profile.

Any pixel in these images is about  $110\mu\text{m}$  by  $110\mu\text{m}$  in size. This resolution is limited by the natural divergence of the neutron beam, the inherent resolution of the scintillator and the optical system. The greylevels are known within a relative error of about  $\Delta c/c \approx 6 \cdot 10^{-4}$  per pixel. For this precision the images were summed from 1000 pictures of each  $200\mu\text{s}$  exposure time.

By summing the density distribution  $\int \mu(x, y, z) dz$  along the  $y$ -axis perpendicular to the neutron beam and acknowledging the implicit projection along the  $z$ -axis an attenuation profile  $\mu(x)$  is created, see figure 8.

It is necessary to correct for some scattering effects. Scattered neutrons from all over the sample contribute to the brightness of the image near the centre; however scattered neutrons only from one half space of the sample contribute to the brightness of the border. That is why a homogenous sample with significant scattering looks brighter in the centre than at its borders.

The detection of scattered neutrons also decreases the overall observed attenuation, which is considerably lower than the anticipated  $\mu_{steel} = 1.2\text{ cm}^{-1}$ . Both corrections, for the gradient and the overall shift, yield the corrected attenuation profile shown in figure 9.

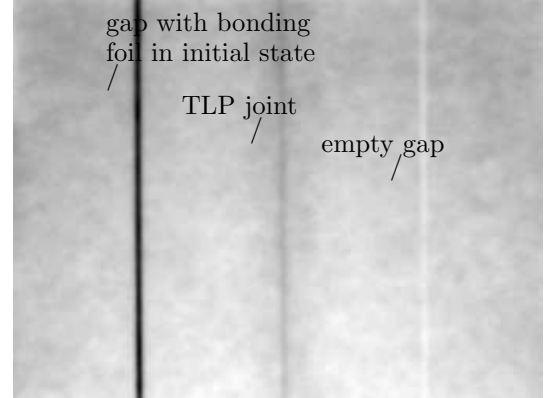


Fig. 7: region of interest

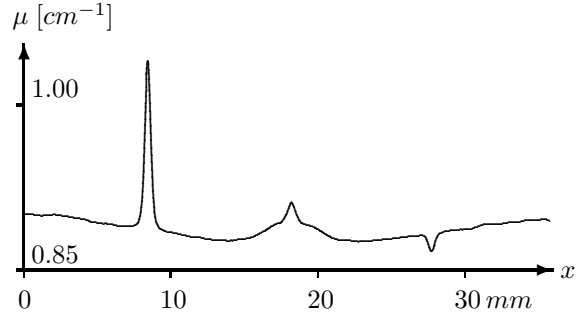


Fig. 8: attenuation profile

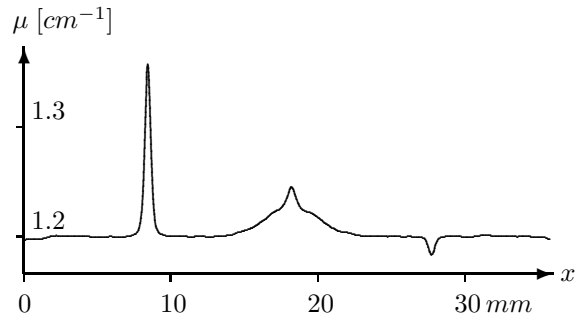


Fig. 9: attenuation profile, corrected for scattering effects

## VI. EVALUATION AND INTERPRETATION

The corrected diffusion profile shows three distinct features:

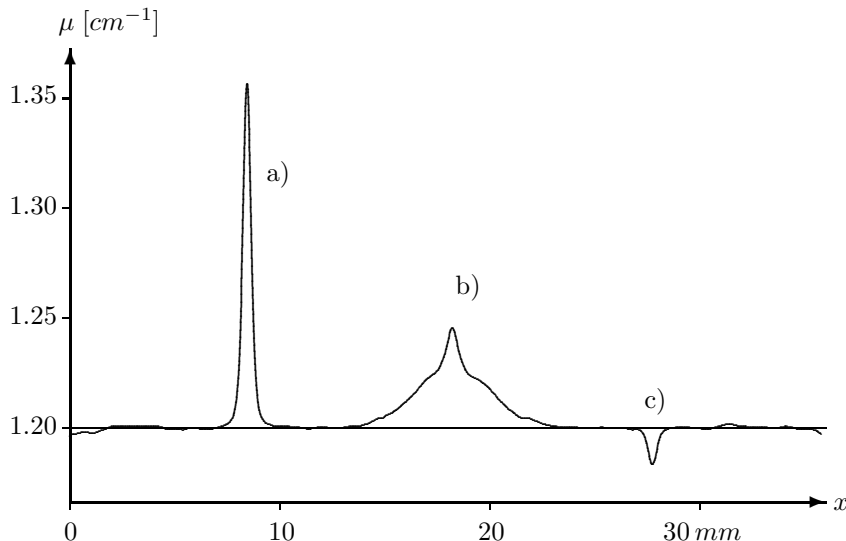


Fig. 10: corrected attenuation profile (enlarged)

a)

At  $x \approx 28\text{mm}$ , there is a dip in overall attenuation. This dip is at the position of the right gap. In fig. 7 this gap appears lighter than the surrounding material. The drop in attenuation is caused by the gaps between the adjacent surfaces. As the surfaces are only level to a scale of about  $15\mu\text{m}$  there are tiny hollow gaps of the same size between the two steel blocks. They are filled with air which features an attenuation which is negligible to that of steel. The spread of the peak is due to the limited accuracy to which the sample has been rotated perpendicular to the beam (projection effect), to the divergence of the neutron beam (blurring the image) and the finite resolution of the optical system.

b)

At  $x \approx 9\text{mm}$ , there is a sharp peak in overall attenuation. The corresponding left gap is visible as a sharp dark vertical line in fig. 7. This gap contains a bonding foil of  $50\mu\text{m}$  width. The low level of neutron transmission of the line is due to the higher boron content in the foil. Boron is highly visible in neutron radiography because of its large neutron capture cross-section. The measured attenuation coefficient is lower than the calculated value, again because of detection of scattered neutrons. Also, the point spread function of the detector is wider than  $50\mu\text{m}$  thus blurring the peak.

c)

Finally, the peak at  $x \approx 18\text{mm}$  is from the TLP bond. The attenuation profile shows a peak as wide as that of the foil in the left slit but less high, accompanied by a much wider diffusion-like curve. On the radiography image in fig. 7 the middle vertical line indicates the position of the final TLP bond. The faint grey line is as wide as the left line but less dark. It is surrounded by a broad halo indicating the diffused boron.

The findings lead to the following observations and conclusions:

The boron has not been dissolved completely. Part of it remained at its initial position and produced the narrow middle peak. It is smaller however than that of the left slit as most of the material in fact has diffused into the surrounding metal.

The dynamics of this diffusion are governed by Fick's second law  $dc/dt = D(T) \cdot d^2c/dx^2$  where  $c$  is the concentration and  $D(T)$  is the temperature dependent diffusion coefficient. Two solutions to this equations describe the state after the first and second stage of the bonding process [10]:

As the foil did not dissolve completely, it resembled a reservoir at  $x = 0$ . In this case the solution to Fick's law is

$$c \sim e^{-(x/(2\sqrt{D(T)t}))^2}$$

In fact, the diffusion profile of the center bond, is perfectly fitted by this curve with a characteristic length scale of  $x_0 = 2\sqrt{D(T)t} = 2.4mm \pm 0.1mm$ :

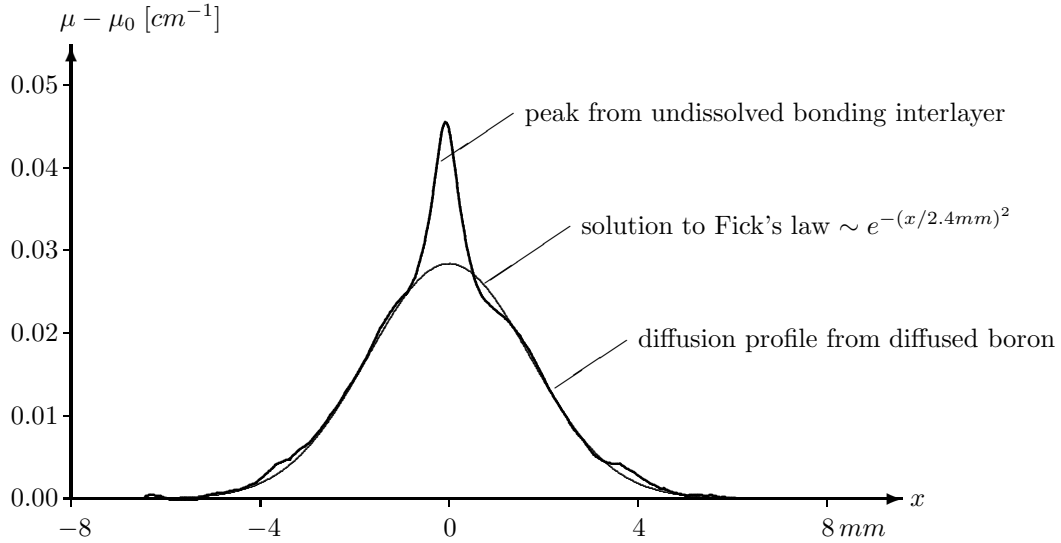


Fig. 11: attenuation profile and Gaussian fit

When comparing the area under the diffusion curve to the total area under the attenuation profile of the middle peak, one finds that about  $90\% \pm 5\%$  of the boron has diffused into the base material.

While the interlayer dissolves quickly into the liquid phase, this phase expands by outward diffusion of the additives leading to further solution of the solid base material. One could ideally assume that at the beginning of the second stage of the bonding process there had been a step in concentration at the liquid-solid interface at  $x_{LS}$ . In this case the solution to Fick's law was

$$c \sim 1 - \frac{2}{\sqrt{\pi}} \int_0^{(x-x_{LS})/(2\sqrt{D_{LS}(T)t})} dy \exp(-y^2)$$

This curve does not fit the data as well as the Gaussian curve did, but the position of the liquid-solid interlayer can be estimated as  $x_{LS} \approx \pm 2.2mm$  which is on a similar lengthscale as  $x_0 \approx x_{LS}$ . As expected, diffusion is much slower here with  $D_{LS}(T) \cdot t \approx 0.2 \dots 0.4 mm^2$  as compared to  $D(T) \cdot t = 1.44 mm^2 \pm 0.12 mm^2$  within the liquid. In any case, the multiple of diffusion coefficient and time is way too low for a complete diffusion of the interlayer and subsequent leveling of the gradient in concentration of the additives.

From the experimental evidence it appears that the specimen resembles an imperfect joint created in an incomplete bonding process. This assumption is supported by the incompletely diffused boron as seen from the undissolved center peak, as well as from the low value for  $D(T) \cdot t$  hinting to an insufficient diffusion time  $t$  or a low diffusion coefficient  $D(T)$  caused by a too low temperature  $T$ .

## VII. CONCLUSION AND OUTLOOK

Using non-destructive neutron radiography we have visualised a TLP bonding joint and determined the diffusion profile of the boron contained in the bonding additives. From this profile we were able to quantitatively determine parameters of the bonding process and to qualitatively show that the joint had not been made using the optimum process parameters.

Between 5% and 15% of the boron did not resolve, in contrast to the theoretical expectation of complete diffusion. The remaining 85% to 95% of the boron diffused into the surrounding metal with a characteristic diffusion length of  $2.4\text{mm} \pm 0.1\text{mm}$  corresponding to a multiple of diffusion coefficient and diffusion time of  $D(T) \cdot t = 1.44\text{mm}^2 \pm 0.12\text{mm}^2$ . The diffusion through an idealized liquid-solid interface took place at surfaces  $2.2\text{mm}$  apart from the center with a multiple of  $D_{LS}(T) \cdot t \approx 0.3 \pm 0.1$ .

From these results it is obvious that the sample features an imperfect TLP joint due to a too low temperature or a too short time at temperature for the interlayer to diffuse completely. In fact, it was revealed only ex post that the specimen was processed at a temperature below the recommended brazing temperature. This fact and further details of the bonding process below were revealed only after the completion of the experiment and the evaluation of the data. Thereby we show that neutron radiography was able to detect the imperfectness of the joint.

The sample under investigation was produced as part of a trial to optimise the process parameters of TLP bonding in terms of brazing temperature and time at temperature. The parameters used for the bonding of the sample under investigation were the least effective ones compared with higher temperatures at the same time or longer times at the same temperature. This is supported by complementary methods including tensile and toughness and SEM micrographs - which fully reflects the non destructive findings that this was not an ideal TLP joint.

This observation highlights the efficacy of neutron radiography for non destructive examination of TLP bonded joints as it clearly shows that the bond has failed to achieve completion. These results are also evidence of the fact that neutron radiography begins to move towards quantitative applications. Already now, neutron radiography and neutron tomography are proven methods in many aspects of materials science and beyond. We hope to trigger further interest in this rapidly developing technique and its applications. Further progress may be expected in a number of areas:

Given the rate of data acquisition available on Neutrograph it could even show the time-resolved dynamics of the bonding process. The different stages of TLP bonding processes take place on timescales between seconds and hours. A neutron radiography is produced from several images taken with an exposure time of some ten milliseconds at our high flux installation. Therefore it will be possible to resolve the kinematics of a bonding process both in space and time. Contrast and hence statistics and time resolution can be enhanced by substituting the boron in the bonding foil by the highly attenuating isotope  $^{10}\text{B}$ .

Even more information could be extracted by using neutron tomography, in particular for non-flat specimen geometries. As in medical computer tomography the three dimensional structure of an object is reconstructed from two dimensional projections. Neutron tomography has successfully produced reconstructions of objects featuring a very low contrast [11]. This is especially suitable for late stages of the bonding process where large time scales enable high counting statistics. On the other hand, high speed neutron tomography is currently under development and could even resolve the fast dynamics of the first stages of a TLP bonding process.

To summarize, we have non-destructively studied a TLP bonding joint. We are developing a reliable method which will provide quantitative, three dimensional, time resolved data of TLP bonding processes. This data will enable materials science to develop a better understanding of the bonding process and a further optimization of its parameters (composition of the foil, temperature curve, ...). We have also shown that this method can be used in non-destructive testing to detect incomplete bonding processes. Finally it also provides difficult to obtain validation data for theoretical modelling of diffusion processes in metals.

## VIII. ACKNOWLEDGEMENT

The sample was made by The Welding Institute in Abington, UK. It was provided through the Sheffield Hallam University and the FaME38 Collaboration at the Institut Laue-Langevin. The Neutrograph experiment is run in collaboration between the Institut Laue-Langevin and the University of Heidelberg. It has been funded by the German Federal Ministry for Research and Education under contract number 06HD153I.

---

\* Electronic address: ballhausen@physi.uni-heidelberg.de

- [1] J. P. Barton, P. von der Hardt (ed.):  
*Proc. 1st World Conference on Neutron Radiography*  
D. Reidel Publishing Co., Dordrecht, 1983
- [2] E. H. Lehmann:  
*Neutron Imaging*  
Proc. 18th Summer School on Neutron Scattering, Zuoz (2000)
- [3] B. Schillinger:  
*Neutron Tomography*  
Proc. 18th Summer School on Neutron Scattering, Zuoz (2000)
- [4] A. Hillenbach, M. Engelhardt, H. Abele, R. Gähler:  
*High flux neutron imaging for high-speed tomography, dynamic tomography and strongly absorbing materials*  
Nuclear Instruments & Methods in Physics Research A 542 (2005) 116-122
- [5] W. D. MacDonald, T. W. Eagar:  
*Transient Liquid Phase Bonding Processes*  
Annual Review of Materials Science 22 (1992) 23-46
- [6] [www.msm.cam.ac.uk/mmc/research/liq\\_ph\\_bond/lpb.html](http://www.msm.cam.ac.uk/mmc/research/liq_ph_bond/lpb.html):  
*Numerical modelling and experimental investigations of transient liquid phase phenomena*  
[...] data of TLP bonding experiments are sparse. Generally, measurements are performed by interrupting a bonding cycle after a certain time to take a cross-section through a sample and directly measuring the thickness of liquid under a microscope. Generating results in this way is labour intensive and only gives pointwise data; in addition, composition profiles are difficult to obtain. [...]
- [7] M. Schneider:  
*Studies for neutron tomography at the Institut Laue-Langevin*  
diploma thesis, University of Heidelberg, 2001
- [8] P. Vontobel, E. H. Lehmann:  
*Measurement of the boron distribution and content of aluminium and stainless steel plates by thermal neutron radiography*  
PSI-Annual-Report 1999, Annex VI, p. 61
- [9] B. Schillinger, Chr. Rausch:  
*High-performance neutron detector for radiography and small-angle scattering: Neutron detection with astronomical CCDs*  
SPIE 2198-160, pp. 974-978 (1994)
- [10] R. E. Smallman, R. J. Bishop:  
*Modern Physical Metallurgy and Materials Engineering*  
Elsevier
- [11] H. Ballhausen, H. Abele, R. Gähler, A. van Overberghe:  
*Low Contrast Neutron Tomography*  
paper in preparation